ANALYSIS OF AIRBORNE IMAGING SPECTROMETER DATA FOR THE RUBY MOUNTAINS, MONTANA, BY USE OF ABSORPTION-BAND-DEPTH IMAGES

DAVID W. BRICKEY, JAMES K. CROWLEY, and LAWRENCE C. ROWAN,
U.S. Geological Survey, Mail Stop 927, Reston, Virginia 22092

ABSTRACT

Airborne imaging spectrometer-1 (AIS-1) data were obtained for the Ruby Mountains of southwestern Montana, an area of amphibolite-grade metamorphic rocks that have moderate rangeland vegetation cover. Although rock exposures are sparse and patchy at this site, soils are visible through the vegetation and typically comprise 20-30 percent of the surface area. Channel-averaged low-pass spatially filtered data were used to construct band-depth images for diagnostic soil/rock absorption bands. Sets of three such images were combined to produce color-composite band-depth images. This relatively simple approach did not require extensive calibration efforts and was effective for discerning a number of spectrally distinctive rocks and soils, including soils having high talc concentrations. The results show that the high spectral and spatial resolution of AIS-1 and future sensors holds considerable promise for mapping mineral variations in soil, even in moderately vegetated areas.

INTRODUCTION

The Ruby Mountains in southwestern Montana are underlain by Precambrian metasedimentary rocks. Many different lithologies are present, including dolomitic and calcitic marbles, hornblende gneiss, as well as other varieties of gneiss and schist, volcanic flows, diabase dikes, and alluvium (Heinrich, 1960). Numerous mineral species having diagnostic near-infrared spectral absorption features occur in the area (Table 1). The rangeland vegetation, including grasses, forbs, and shrubs, comprise 70-80% of the surface cover, soils the other 20-30%.

The chief objectives in selecting this study area were to assess the use of AIS-1 data for detecting minerals present in metamorphic rocks and to develop image processing techniques for dealing with moderate amounts of rangeland vegetation and limited rock exposures. Absorption-band-depth (ABD) images provided a relatively simple but effective approach for identifying a number of rocks and minerals present along the AIS-1 flight lines.

DATA COLLECTION AND ANALYSIS

Four flight lines of AIS-1 data were acquired in July 1985 covering approximately 100 km of groundtrack. This paper focuses on a portion of

one of the flight lines, nearly 6-km in length along an area with about 300 m of relief, which was sampled intensively during August 1986. Figure 1 is a geologic map for the area covered by the 6 km data set.

Table 1. AIS-1 wavelengths used in generating ABD images

Channel Combination	Wavelength		Minerals detected
1	2.151-2.179 μm	shoulder 1	Dolomite, talc, tremolite, Mg-mica
	2.347-2.366 μm	shoulder 2	
	2.300-2.319 μm	minimum	
2	2.328-2.347 μm	shoulder 1	Talc, tremolite, Mg-mica
	2.394-2.403 μm	shoulder 2	
	2.366-2.384 μm	minimum	
3	2.123-2.142 μm	shoulder 1	Illite, muscovite, illite/smectite, vermiculite, kaolinite
	2.263-2.282 μm	shoulder 2	
	2.189-2.207 μm	minimum	
4	2.291-2.310 μm	shoulder 1	Calcite, antigorite
	2.366-2.384 μm	shoulder 2	
	2.338-2.347 μm	minimum	
5	2.263-2.282 μm	shoulder 1	Dolomite, talc, tremolite, Mg-mica
	2.347-2.366 μm	shoulder 2	
	2.319-2.328 μm	minimum	
6	2.328-2.338 μm	shoulder 1	Talc, tremolite
	2.366-2.384 μm	shoulder 2	
	2.347-2.366 μm	maximum	
7	2.133-2.151 μm	shoulder 1	Same minerals as channel 3 above
	2.198-2.217 μm	minimum	

The AIS data were vertically de-striped and normalized for topographic and albedo effects by using an equal energy procedure (Jet Propulsion Laboratory, 1985). A 3x3 box filter was then applied to reduce high-frequency noise in the spatial dimension. A relative reflectance data set was generated from the box-filtered data by using the whole-image average spectrum as a divisor. ABD images were produced by using 2 to 3 channels from both shoulders and 2 to 3 channels from the minimum of each absorption feature so as to increase the signal to noise. The sum of all the channels for the shoulders was divided by the sum of the channels for the minimum to produce an ABD image. Table 1 lists the wavelengths of channels used in constructing the ABD images.

RESULTS AND DISCUSSION

Figure 1 is an index map to be used in conjunction with color slides nos. 3 and 4 located in the pocket at the end of the proceedings. The first slide is a color-composite ABD image generated

from the box-filtered AIS data by use of channel combinations 1, 2, and 3 in table 1 as red, green, and blue (RGB), respectively. Note that combinations 1 and 3 both utilize channels that are widely separated in wavelength to define the band shoulders. This slide is referred to henceforth as the "wide-band" image. The second slide uses channel combinations 4, 5, and 2, as RGB (table 1) and is referred to as the "narrow-band" image. This second image was generated from the box-filtered relative reflectance data set.

Comparing the wide-band with the narrow-band images reveals several differences that merit explanation. Site A (fig. 1) on the wide-band image shows a pronounced orange anomaly that is completely absent in the narrow-band image. The anomaly results from high digital number (DN) values in the dolomite and MgOH images (channel combinations 1 and 2, table 1). However, there is no dolomite at this location. Instead, the high DN values probably result from a soil rich in Mg-mica and an especially heavy rangeland vegetation cover. The vegetation gives an anomalous "dolomitic" component in the wide-band image, which is eliminated in the narrow-band image. Figure 2 illustrates schematically that without a continuum removal, a vegetation spectrum appears to have an absorption feature at 2.32 μm. This highlights a general problem in the use of widely separated channels to define absorption band shoulders--the resulting ABD images may lose their specificity for distinguishing materials. On the other hand, because the spectral content is less constrained, wide-band images show more spatial detail over the entire image area. Narrow-band images tend to be spectrally flat, except for local areas that exhibit the absorption features defined by the channel selections.

Sites B and C (fig. 1) contain exposures of calcitic and dolomitic marble, respectively. The principal absorption band centers for these units are offset by only 20 nm and thus provide a fairly rigorous test of AIS spectral discrimination. The wide-band image does not discriminate successfully between the two carbonate minerals. However, the narrow-band image generated from the box-filtered relative reflectance data does separate the calcitic (orange pixels) from the dolomitic minerals (yellow-green pixels). AIS relative reflectance spectra for pixel blocks at sites B and C are shown in figure 3. Also shown in the figure is an AIS relative reflectance spectrum for site D, which had substantial amounts of talc in the soil. The diagnostic talc absorption band at 2.38 μm is apparent in the site D spectrum, as is the MgOH band near 2.31 μm, located essentially at the same wavelength as the major absorption band for dolomite. Because only a few AIS channels are suitable for defining the narrow 2.38-μm feature, separating talc from dolomite provides a rigorous test of the band-depth approach. An ABD image was made by use of a larger number of channels to examine the talc maximum in reflectance near 2.34 μm (table 1, channel 6). However, this feature is not very distinct in the natural soils and the image showed no improvement. Sites E and F (fig. 1) are tremolite-bearing dolomitic marble units that produce a talc-like signature on the two composite ABD images. Talc and tremolite are very similar in the 1.2- to 2.4-μm wavelength range covered by the AIS data and cannot be distinguished; however, they are separable in the 0.4- to 1.2-μm region.

Laboratory spectra for soils in the study area exhibit considerable spectral variation in the 2.1- to 2.4-μm wavelength range. However, because the absorbing soil minerals generally are intermixed with spectrally featureless quartz and feldspar impurities, the spectral differences between soils as seen in the noisy AIS-1 data are very subtle. For example, the most pronounced talc absorption feature shown in laboratory spectra for talc-rich soils collected from site D (fig. 1) has a total band depth of less than 5 percent reflectance. Because the ABD images were able to distinguish features having such low spectral contrast, it appears likely that improved signal to noise will eventually permit other soil types to be detected in areas that have comparable rangeland vegetation cover. Images were produced to examine soil AlOH absorption bands near 2.2-μm (table 1, channels 3 and 7); however, only broad surface areas exhibiting weak absorption were discernable (site G; fig. 1). The strongest 2.2-μm features were observed for a well-exposed, weathered, feldspar-rich pegmatite, shown in the wide-band image at site H (fig. 1).

Simple ratios of channels or groups of channels may be better suited for resolving some spectral features. Laboratory spectra for many soils collected in the study area produced 2.2-μm AlOH absorption bands that lacked a strong rise from the band center to longer wavelengths. This characteristic shape probably was caused by the presence of vermiculite in many soil samples. Channel combination 7, a ratio image of one set of channels divided by another set, improved discrimination of this type of feature. Because of the mineralogical complexity of the soils in the study area, it would have been difficult to predict the form of the 2.2-μm soil feature without field sampling.

CONCLUSIONS

Absorption-band-depth images created from relative reflectance AIS-1 data provide a simple but effective approach for distinguishing some metamorphic rocks and minerals. The use of such images requires that assumptions be made regarding the absorption features present in a study area. Such assumptions can be misleading, especially in situations involving complex mineral mixtures that produce unfamiliar spectral reflectance curves. On the other hand, narrow ABD images are extremely specific and may facilitate the digital enhancement of subtle soil spectral features in rangeland-type vegetated areas.

REFERENCES

Heinrich, E.W., 1960, Geology of the Ruby Mountains and nearby areas in southwestern Montana: in Pre-Beltian Geology of the Cherry Creek and Ruby Mountains Areas, Southwestern Montana: Montana Bureau of Mines and Geology Memoir 38, p. 15-40.

Jet Propulsion Laboratory, 1985, Science Investigators Guide to AIS Data: Jet Propulsion Laboratory, Pasadena, California, p. III-2.

Acknowledgments: The authors would like to thank Fred Kruse and Dennis Krohn for their assistance and sharing of software used to process the AIS data in this study.

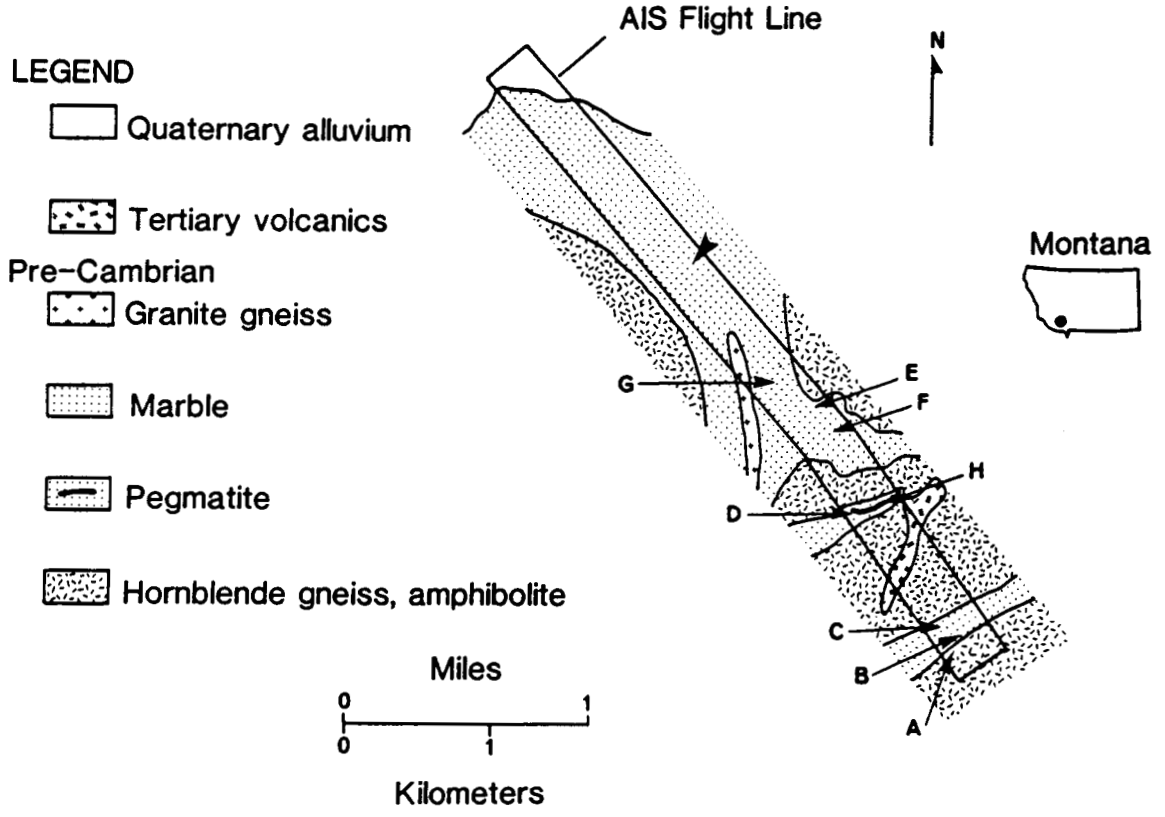

Figure 1. Geologic map of the Ruby Mountains study area. The lettered arrows indicate field sites that are discussed in the text. Also refer to slide nos. 3 and 4, located in the pocket at the end of these proceedings. The large arrow shows the northwest limit of the slide coverage. After Heinrich (1960).

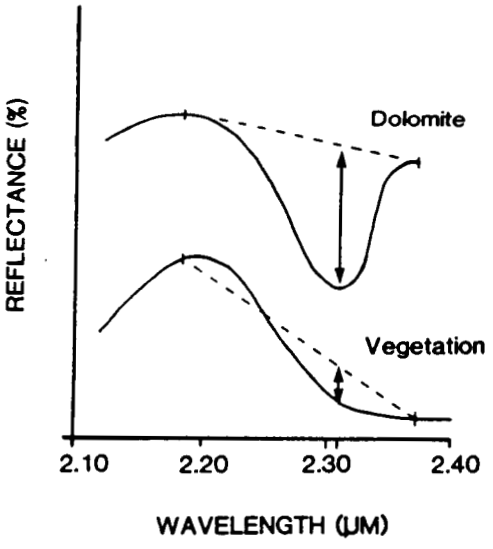

Figure 2. Schematic diagram showing the apparent "dolomite" component produced by rangeland vegetation in a band depth image in which separated shoulder channels were used.

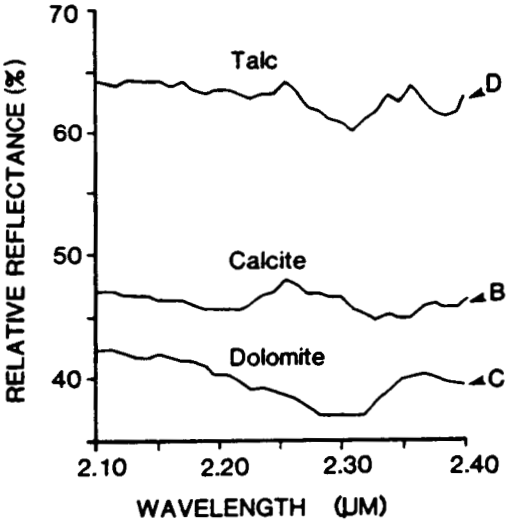

Figure 3. AIS spectra produced from the relative reflectance data set for field sites B, C, and D (refer to fig. 1).